nature electronics

Article

https://doi.org/10.1038/s41928-023-00931-1

Small-voltage multiferroic control of two-dimensional magnetic insulators

Received: 4 December 2021

Accepted: 27 January 2023

Published online: 06 March 2023

Check for updates

Shanchuan Liang[1], Ti Xie[1], Nicholas A. Blumenschein[2], Tong Zhou[3], Thomas Ersevim[4], Zhihao Song[1], Jierui Liang[1], Michael A. Susner[5], Benjamin S. Conner[6,7], Shi-Jing Gong[8], Jian-Ping Wang[9], Min Ouyang[4], Igor Žutić[3], Adam L. Friedman[2], Xiang Zhang[10] & Cheng Gong[1]

Magnetic insulators, which have long-range magnetic order and are electrically insulating, allow spin propagation without electron motion and could be used to create dissipationless magnetoelectric and magneto-optical devices. Atomically thin two-dimensional (2D) magnetic insulators could, in particular, be used to fabricate compact devices. However, the efficient electrical control of 2D magnetic insulators remains a challenge due to difficulties in electrostatically doping such insulators and the inability of external electric fields to modify their crystal fields. Here we report the electrical control of the 2D magnetic insulator chromium germanium telluride ($Cr_2Ge_2Te_6$) using a thin ferroelectric polymer. We show that ±5 V across the $Cr_2Ge_2Te_6$/polymer heterostructures can open and close the magnetic hysteresis loop. The magnetic modulation is non-volatile, and is observed in bilayer, trilayer and four-layer $Cr_2Ge_2Te_6$, but not in thicker eight-layer $Cr_2Ge_2Te_6$, which indicates the importance of the interfacial multiferroic effect. The heterostructure multiferroics also enable direct electrical toggling between two magnetization states.

Magnetic insulators (MIs) allow spin-wave propagation whereas forbid charge current. They, thus, provide a class of platforms for the development of energy-efficient spintronic and magnonic devices that separate the flow of spin and charge[1,2]. The MI yttrium iron garnet offers ultralow Gilbert damping constants on the order of 10^{-5} and ultralong magnon diffusion lengths of tens to hundreds of micrometres, which are enabled by the suppressed electron–magnon scattering[3,4]. Alternatively, the MI terbium gallium garnet offers efficient optical isolation, which is enabled by the strong Faraday effect[5] with high optical transparency[6,7]. These examples highlight the unique magnetoelectric and magneto-optic effects of MIs that can be used to create niche devices[8–12].

The discovery of two-dimensional (2D) layered MIs—such as chromium germanium telluride ($Cr_2Ge_2Te_6$) and chromium triiodide (refs. [13,14])—could lead to the development of new applications due to their atomic thinness, wide property tunability and simple construction of van der Waals heterostructures[15–18].

Efficient voltage control of 2D MIs is critical for applications. The electrical control of magnetism has been demonstrated in diluted magnetic semiconductors[19,20], metal thin films[21,22] and 2D magnets[23–25]. However, the efficiency needs to be improved. The low controlling efficiency is linked to two fundamental issues: external electric fields are typically three orders of magnitude weaker than materials' crystal fields, and

[1]Department of Electrical and Computer Engineering and Quantum Technology Center, University of Maryland, College Park, MD, USA. [2]Laboratory for Physical Sciences, College Park, MD, USA. [3]Department of Physics, University at Buffalo, State University of New York, Buffalo, NY, USA. [4]Department of Physics, University of Maryland, College Park, MD, USA. [5]Materials and Manufacturing Directorate, Air Force Research Laboratory, Wright-Patterson Air Force Base, Dayton, OH, USA. [6]Sensors Directorate, Air Force Research Laboratory, Wright-Patterson Air Force Base, Dayton, OH, USA. [7]National Research Council, Washington DC, USA. [8]Department of Physics, School of Physics and Electronic Science, East China Normal University, Shanghai, China. [9]Department of Electrical and Computer Engineering, University of Minnesota, Minneapolis, MN, USA. [10]Faculty of Science and Faculty of Engineering, The University of Hong Kong, Hong Kong, China. e-mail: gongc@umd.edu

https://doi.org/10.1038/s41928-023-00931-1

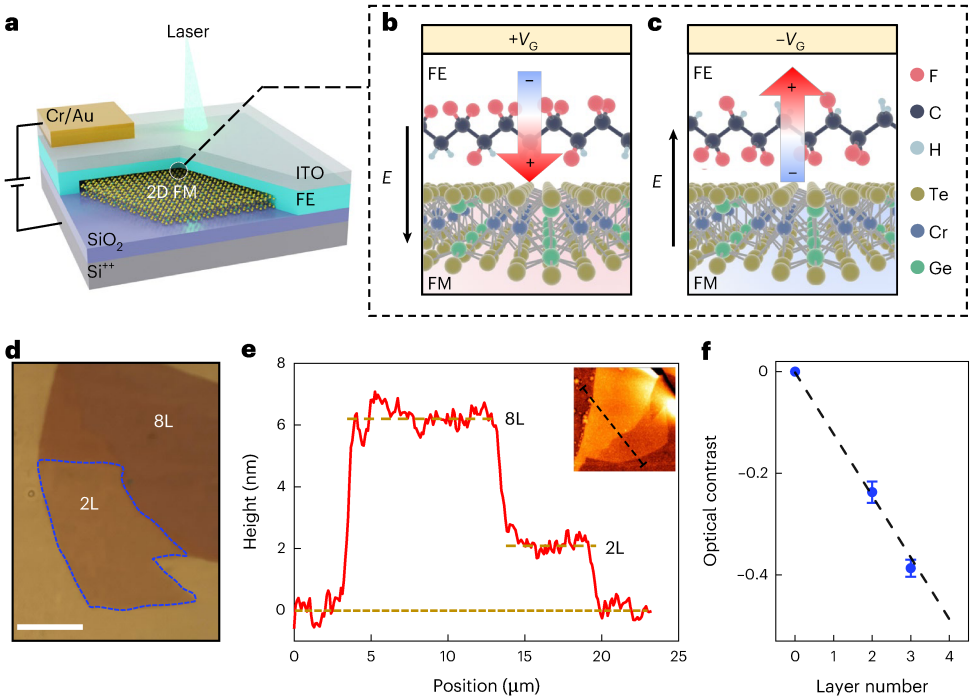

Fig. 1 | Multiferroic heterostructure device. a, Schematic of a $Cr_2Ge_2Te_6$/P(VDF-TrFE) multiferroic heterostructure sandwiched between the top electrode (ITO/Au) and 260-nm-thick SiO_2/Si substrate. **b**,**c**, Side views of two configurations of the multiferroic heterostructure under a positive (**b**) and negative (**c**) gate voltage. When FE P(VDF-TrFE) is oppositely polarized, the interfacial couplings differ, as indicated by the detailed interfacial atomic configurations (for example, hydrogen atoms are in direct contact with $Cr_2Ge_2Te_6$ in **b**, but not in **c**). The red- and blue-shaded areas represent $Cr_2Ge_2Te_6$ under down- and up-polarized P(VDF-TrFE), respectively. **d**, Optical image of the as-exfoliated 2L- and 8L-$Cr_2Ge_2Te_6$ (scale bar, 5 μm). **e**, AFM line profile of the 2L- and 8L-$Cr_2Ge_2Te_6$ flakes. The inset shows the AFM image and line-scan position (black dashed line). The AFM-measured step height for 2L-$Cr_2Ge_2Te_6$ is larger than 1.4 nm due to the possible moisture and air gap between the exfoliated 2D flake and SiO_2 substrate[33]. **f**, Layer-dependent optical contrasts extracted from optical images of 2L- and 3L-$Cr_2Ge_2Te_6$ flakes, which follow the linear dependence on layer numbers. The error bars represent the standard deviation from the mean of the statistical analysis of the optical contrast under three repetitive measurements.

electrostatic doping via conventional dielectric gating can only achieve a fractional modulation of electron population (0.001–0.010 electrons per surface atom). Multiferroics[9,26,27] have an inherent coupling between ferroelectric (FE) order and ferromagnetic order and could transform external voltages into drastic alternation of the internal crystal fields. However, creating single-phase 2D multiferroics requires addressing the dual challenges of enhanced thermal fluctuations in 2D ferromagnets (FMs) and enhanced depolarization fields in 2D FEs[28–30]. Heterostructure multiferroics could potentially mitigate these challenges and allow the versatile interfacial engineering of 2D multiferroicity.

In this Article, we report a multiferroic heterostructure that consists of 2D MI $Cr_2Ge_2Te_6$ and the FE polymer poly(vinylidene fluoride-co-trifluoroethylene) (P(VDF-TrFE)) (refs. [31,32]). The magnetic hysteresis loop of 2D $Cr_2Ge_2Te_6$ can be effectively opened and closed by applying small voltages of ±5 V across the heterostructure, indicating a modulation of magnetic anisotropy. In particular, a hysteresis loop with coercivity of 5 mT and 14% remanent magnetization can be reversibly created and annihilated by applying ±5 V. The modulation effects remain after voltages are withdrawn, showing clear non-volatility. The behaviour is observed in bilayer (2L), trilayer (3L) and four-layer (4L) $Cr_2Ge_2Te_6$, but not in thicker eight-layer (8L) $Cr_2Ge_2Te_6$, suggesting that interfacial coupling plays a critical role in the mechanism. Furthermore, by sweeping the voltage, a direct toggling between two magnetization states is achieved in a 2L-$Cr_2Ge_2Te_6$ heterostructure kept at a constant magnetic field of ±9 mT with transition voltages of ±5 V.

Multiferroic heterostructure devices

The vertically stacked multiferroic heterostructures comprise the 2D FM $Cr_2Ge_2Te_6$ and the FE polymer P(VDF-TrFE), sandwiched between a SiO_2/Si substrate and a top electrode (Fig. 1a). The 2D $Cr_2Ge_2Te_6$ flakes were mechanically exfoliated from bulk $Cr_2Ge_2Te_6$ crystals onto 260 nm SiO_2/Si substrates (Methods), followed by the spin coating of 50-nm-thick P(VDF-TrFE), which protects 2D $Cr_2Ge_2Te_6$ from ambient degradation. The top electrode consists of a global 20-nm-thick transparent indium tin oxide (ITO) that allows the probing laser to access the 2D magnet for reflectance magnetic circular dichroism (RMCD) study, and a local metallic contact (Cr (5 nm) and Au (50 nm)) through which voltages are applied. The p-doped Si serves as the bottom electrode. The optical image of a 2L-$Cr_2Ge_2Te_6$ flake is circled by the blue dashed lines with an adjacent 8L flake on the top right (Fig. 1d). The thickness of the few-layer $Cr_2Ge_2Te_6$ is confirmed by atomic force microscopy (AFM)[33] and optical contrast (Fig. 1e,f) measurements.

Interfacial coupling mechanisms

Two configurations of the $Cr_2Ge_2Te_6$/P(VDF-TrFE) multiferroic heterostructure are depicted (Fig. 1b,c) when the FE polarization vector of P(VDF-TrFE) points downward (↓) and upward (↑) in response to positive and negative voltages, respectively. The interfacial atomic configurations under the opposite FE polarizations are distinct: hydrogen atoms are present at the interface in the downward-polarized case (Fig. 1b) but absent from the interface in the upward-polarized case (Fig. 1c). In these heterostructures, the FEs can affect 2D magnets through three different mechanisms. First, FEs can amplify the external electric field due to their inherent electrical dipoles, which has led to the development of <60 mV dec^{-1} subthreshold swing in FE-gated field-effect transistors[34]. If this field amplification mechanism dominates[28,35], the opposite FE polarizations should cause the same effect on 2D magnets. Second, when FEs are oppositely polarized, the atomic

https://doi.org/10.1038/s41928-023-00931-1

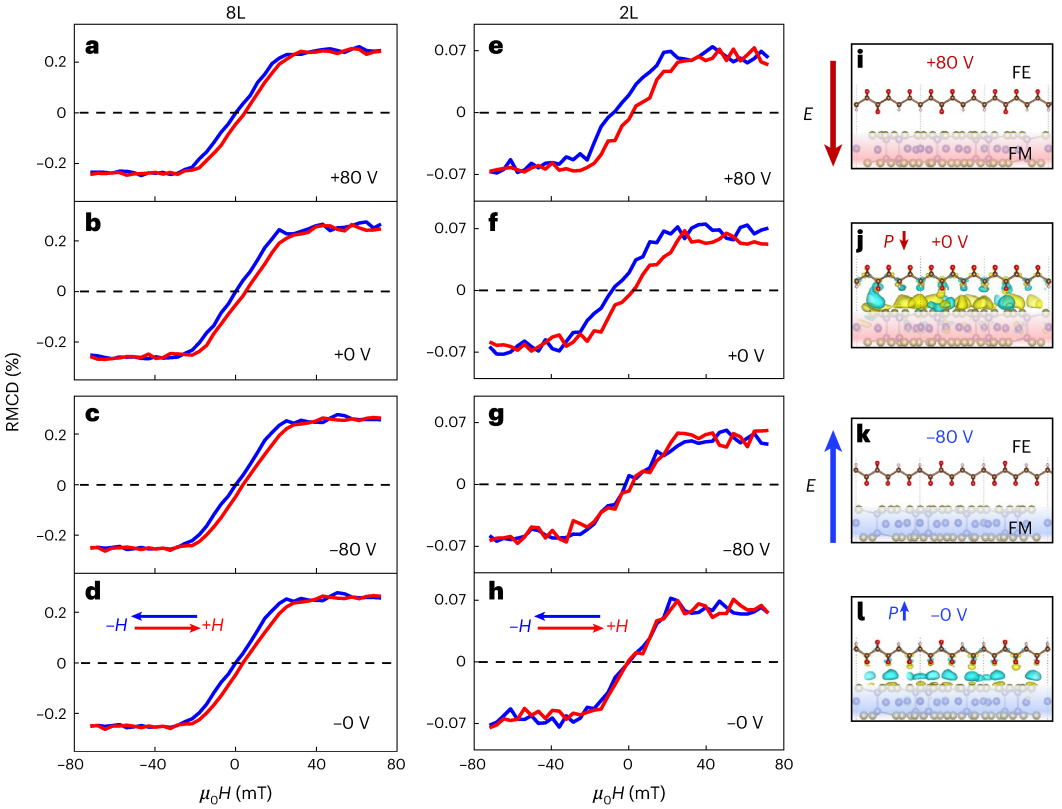

Fig. 2 | Voltage control of magnetism in $Cr_2Ge_2Te_6$/P(VDF-TrFE). a–d, Hysteretic magnetic field dependence of RMCD of 8L-$Cr_2Ge_2Te_6$ under four voltages (+80 (**a**), +0 (**b**), −80 (**c**) and −0 V (**d**)) at 4 K. The hysteresis loops remain almost unchanged under different voltages. **e–h**, Hysteretic magnetic field dependence of RMCD of 2L-$Cr_2Ge_2Te_6$ under the four representative voltages (+80 (**e**), +0 (**f**), −80 (**g**) and −0 V (**h**)). Here +80 V opens a magnetic hysteresis loop with large coercivity, whereas −80 V completely closes the hysteresis loop, corresponding to two switchable magnetic states, namely, ON and OFF. The hysteresis loops at ±0 V remain the same as the previous ON/OFF states at ±80 V (+0 and −0 V mean 0 V is withdrawn from +80 and −80 V, respectively), showing clear non-volatility. Both observations that (1) 8L- and 2L-$Cr_2Ge_2Te_6$ have contrasting responses to the applied voltages and (2) 2L-$Cr_2Ge_2Te_6$ has distinct responses to ±80 V suggest that the interfacial magnetoelectric coupling (rather than the FEs' field amplification mechanism) dominates. **i–l**, Atomic structures and calculated differential charge densities (Supplementary Fig. 2) of the P(VDF-TrFE)/$Cr_2Ge_2Te_6$ heterostructure under opposite FE polarizations (+80 (**i**), +0 (**j**), −80 (**k**) and −0 V (**l**)). The yellow and cyan colours in **j** and **l** represent charge accumulation and depletion, respectively, where the isosurface value is set to 0.0002 electrons $Å^{-3}$. The red- and blue-shaded areas represent $Cr_2Ge_2Te_6$ under down- and up-polarized P(VDF-TrFE), respectively. As shown in **j** and **l**, the difference in wavefunction overlap at the heterostructure interface under opposite FE polarizations (±0 V) is evident, which supports the interfacial hybridization mechanism underlying our experimentally observed multiferroic control of 2D magnetism.

bonding configurations at the multiferroic interface differ (Fig. 1b,c), resulting in different interfacial hybridizations that differently alter the crystal fields of 2D magnets. Third, the FEs of opposite polarizations possess different surface-bound charges and work functions, leading to different amounts of charge doping in adjacent 2D magnets.

Under FE-polarization-dependent interfacial hybridization mechanism and FE-polarization-dependent charge-doping mechanism discussed above, opposite FE polarizations can cause distinct magnetic property changes in 2D magnets. Built-in electric fields, if any, are generated through two interfacial electron behaviours: interfacial charge transfer across FE/2D magnet junctions and/or interfacial wavefunction overlap (thereby causing charge redistribution within the FEs and 2D magnets). Since these two fundamental interfacial behaviours have been covered by the three mechanisms discussed above, their effects will be discussed further in the context of our experimental results without specific reference to the built-in electric field.

Multiferroic control of magnetic hysteresis

We first measured the RMCD of 8L- and 2L-$Cr_2Ge_2Te_6$/P(VDF-TrFE) as the out-of-plane magnetic fields are swept under different applied voltages (Fig. 2a–d,e–h). In this work, all the RMCD measurements were conducted at 4 K, unless specified otherwise. As shown in Fig. 2a–d, 8L-$Cr_2Ge_2Te_6$ shows a ferromagnetic hysteresis loop with coercivity H_C of 2.3 mT, which agrees well with the soft ferromagnetism of $Cr_2Ge_2Te_6$ (ref. [13]). When voltages of +80, +0, −80 and −0 V are applied, the shape of the hysteresis loop and the amplitude of coercivity of 8L-$Cr_2Ge_2Te_6$ remain approximately unchanged. In contrast, 2L-$Cr_2Ge_2Te_6$ exhibits distinct hysteresis loops when ±80 V are applied, respectively: under +80 V, the hysteresis loop is opened with a finite coercive field and remanence, whereas under −80 V, the hysteresis loop completely closes. A similar electrical effect on the hysteresis loop can be observed in 4L-$Cr_2Ge_2Te_6$/P(VDF-TrFE) (Supplementary Fig. 1). The observation that the electrical control is prominent in 2D samples (that is, 2L- and 4L-$Cr_2Ge_2Te_6$) but not in the thick sample (that is, 8L-$Cr_2Ge_2Te_6$) provides strong evidence that the interfacial interactions (including interface hybridization and charge transfer doping) dominate over the field amplification effect, because a pure electric field would penetrate through all the 2L, 4L and 8L flakes and cause similar responses in $Cr_2Ge_2Te_6$ of different thicknesses. Furthermore, in the case of 2D samples, the distinct hysteresis loops measured under opposite voltages (that is, ±80 V) further supports the hypothesis of a dominant role of interfacial magnetoelectric coupling, as opposite electric fields would not cause the observed difference in $Cr_2Ge_2Te_6$.

https://doi.org/10.1038/s41928-023-00931-1

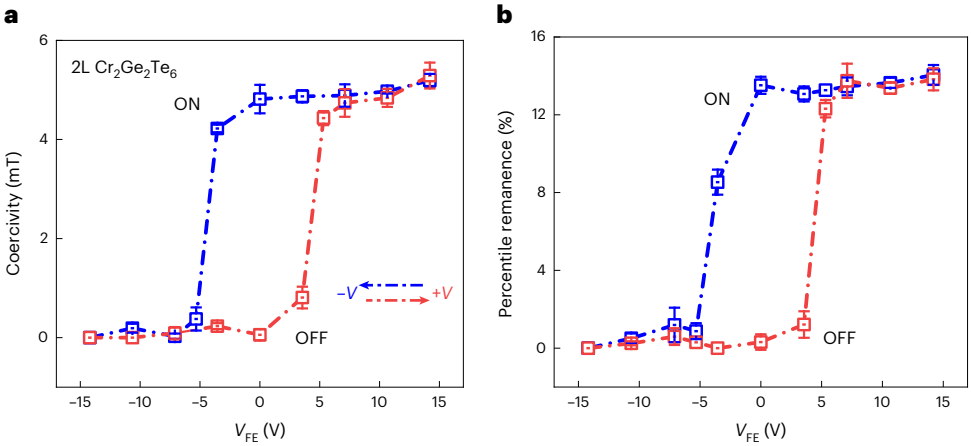

Fig. 3 | Voltage dependence of magnetic coercivity and percentile remanent magnetization in 2L-$Cr_2Ge_2Te_6$/P(VDF-TrFE) at 4 K. a, Magnetic coercivity versus effective voltage V_{EF} dropping only across the 2L-$Cr_2Ge_2Te_6$/P(VDF-TrFE) heterostructure. Each data point is extracted from RMCD-measured magnetic hysteresis loops by systematically sweeping the voltages. The magnetic coercivity of 5 mT is obtained for the ON state. **b**, Percentile remanence as a function of V_{EF}. A percentile remanence of 14% is obtained for the ON state. Both **a** and **b** show similar non-volatile hysteresis characteristics with the flipping effective voltages V_{EF} of ±5 V, at which two magnetic states (ON/OFF) can be reversibly switched back and forth. The error bars represent the standard deviation from the mean of coercivity or percentile remanence derived from the magnetic hysteresis loops under five repetitive measurements.

Density functional theory (DFT) calculations support the dominant role of interfacial hybridization mechanism instead of the charge transfer doping mechanism. Calculations of a model heterostructure of $Cr_2Ge_2Te_6$/P(VDF-TrFE) with opposite FE polarizations show a prominent difference in interfacial wavefunction overlap. The heterostructure with a down-polarized P(VDF-TrFE) has a larger interfacial wavefunction overlap than the same heterostructure with an up-polarized P(VDF-TrFE) (indicated by the larger area of yellow and cyan isosurfaces in Fig. 2j than Fig. 2l). Furthermore, the calculated doping levels in $Cr_2Ge_2Te_6$ induced by the interfacial charge transfer from P(VDF-TrFE) with down and up polarizations are 4.0×10^{12} electrons cm^{-2} and 1.5×10^{12} holes cm^{-2}, respectively (Supplementary Fig. 2). The calculated doping-dependent magnetic anisotropy of 2D $Cr_2Ge_2Te_6$ shows that the abovementioned doping levels (Supplementary Fig. 3, yellow dashed lines) have a negligible effect on the magnetic anisotropy of 2D $Cr_2Ge_2Te_6$. Moreover, we experimentally verified that electrostatically doping $Cr_2Ge_2Te_6$ even up to the density of $\pm 8 \times 10^{12}$ electrons cm^{-2} cannot cause the observed modulation effects in coercivities (that is, the coercivities shown in Supplementary Fig. 4a remain almost unchanged). Therefore, the combination of the calculated doping level in $Cr_2Ge_2Te_6$ (by interfacial charge transfer from the adjacent P(VDF-TrFE)), the calculated doping-dependent magnetic anisotropy of $Cr_2Ge_2Te_6$ and experimentally measured coercivities of the electrostatically doped $Cr_2Ge_2Te_6$ suggest that the interfacial charge doping is not the main underlying mechanism causing our observed ferroelectrically controlled coercivities. Furthermore, the Raman spectra of 2D $Cr_2Ge_2Te_6$ remain unchanged under different voltages (Supplementary Fig. 5), suggesting the absence of observable interfacial strain effect, which would otherwise be common in conventional composite multiferroics[36].

The observed interfacial multiferroic effect is non-volatile. When the magnetic state is ON (that is, the hysteresis loop is opened with non-zero coercivity and remanence; Fig. 2f) at +0 V, the shape of the hysteresis loop, coercivity and remanence are consistent with the previous ON state at +80 V (Fig. 2e). Likewise, for the OFF state (that is, vanishing coercivity and remanent magnetization) by applying −80 V (Fig. 2g), the magnetic hysteresis loop continues to remain in the OFF state after −80 V is removed (that is, −0 V; Fig. 2h). A similar non-volatile effect is reproduced for the 4L-$Cr_2Ge_2Te_6$ device (Supplementary Fig. 1). Non-volatility is a hallmark characteristic of FE electronics with technological significance.

We continue to systematically study the electrical control of the 2L-$Cr_2Ge_2Te_6$ device by sweeping the external voltages with a step size of 20 V (Supplementary Fig. 6). The voltage-dependent coercivity and percentile remanence are summarized in Fig. 3a,b. To quantify the switching behaviours of our multiferroic heterostructures, we estimated the effective voltage across the $Cr_2Ge_2Te_6$/P(VDF-TrFE) heterostructure excluding the voltage drop across the 260-nm-thick SiO_2. We conducted a capacitance–voltage (C–V) measurement of P(VDF-TrFE)/SiO_2 to deduce the relative capacitance ratio between P(VDF-TrFE) and SiO_2, and calculated that the voltage drop across P(VDF-TrFE) is 17.7% of the voltage applied across the entire device (Supplementary Fig. 7). Hereafter, the effective voltage (V_{EF}) denotes the voltage drop across the 2L-$Cr_2Ge_2Te_6$/P(VDF-TrFE) heterostructure.

Both coercivity and percentile remanence show square-shaped electrical hysteresis loops (Fig. 3a,b). The ON and OFF states correspond to the two scenarios when the FEs are polarized downward (↓) and upward (↑), respectively. Specifically, in the case of magnetic coercivity, the V_{EF} value of −5 V is the turning point at which the device switches to the OFF state with vanishing magnetic coercivity. When V_{EF} increases above +5 V, the device switches back to the ON state with a 5 mT magnetic coercivity. Likewise, the percentile remanence (Fig. 3b) exhibits a similar hysteretic dependence on V_{EF}, and switches between 14% (ON) and 0% (OFF) at ±5 V. These results confirm that in this work, ±5 V corresponds to the coercive voltages of the FE P(VDF-TrFE). The coercive electric field of P(VDF-TrFE) of ~100 mV nm^{-1} (that is, 5 V across 50-nm-thick P(VDF-TrFE)) agrees well with previous reports[32]. To further confirm that our calculated V_{EF} value is quantitatively reliable, we fabricated a 3L-$Cr_2Ge_2Te_6$/P(VDF-TrFE) multiferroic device with a graphite bottom electrode on SiO_2 (Supplementary Fig. 8 and Note), which allows us to directly apply voltages across the P(VDF-TrFE)/$Cr_2Ge_2Te_6$ heterostructure by circumventing the voltage dropped across SiO_2 to control the 2D magnetic behaviour. Consequently, the applied small voltages are approximately equivalent to V_{EF}. As shown in Supplementary Fig. 9, based on this device, we indeed demonstrated the non-volatile voltage control of 3L-$Cr_2Ge_2Te_6$ with threshold voltages of about ±5–6 V, which agrees well with our calculated flipping V_{EF} across the P(VDF-TrFE)/$Cr_2Ge_2Te_6$ heterostructure based on SiO_2.

Given that the magnetoelectric ON/OFF behaviours were observed only for 2L-, 3L- and 4L-$Cr_2Ge_2Te_6$ devices (Fig. 2e–h and Supplementary Figs. 1a and 9a) but not in the heterostructure with 8L-$Cr_2Ge_2Te_6$

https://doi.org/10.1038/s41928-023-00931-1

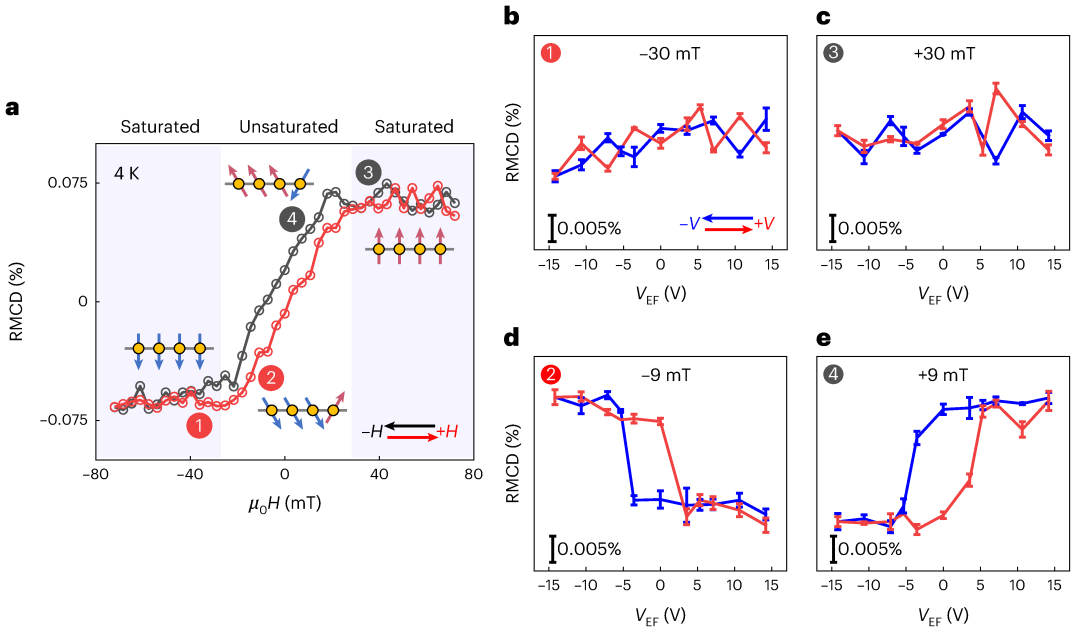

Fig. 4 | Direct voltage switching of magnetization in 2L-$Cr_2Ge_2Te_6$/P(VDF-TrFE). a, RMCD versus magnetic field for 2L-$Cr_2Ge_2Te_6$/P(VDF-TrFE) under the ON state at 4 K. Indexes 1 and 3 represent two conditions in which −30 and +30 mT magnetic fields saturate the magnetization, respectively, and indexes 2 and 4 represent two conditions in which −9 and +9 mT magnetic fields partially magnetize the sample, respectively. **b**,**c**, RMCD at −30 mT (**b**) and +30 mT (**c**) versus effective voltage V_{EF}, corresponding to the initial magnetic saturation states indexed as 1 and 3 in **a**. The RMCD signal shows no observable response to FE manipulation. **d**,**e**, RMCD at −9 mT (**d**) and +9 mT (**e**) versus V_{EF}, corresponding to the initial partially magnetized states indexed as 2 and 4 in **a**. Under static magnetic fields of ±9 mT, repeatable toggling between two magnetization states is observed by sweeping V_{EF}, suggesting an effective FE control of magnetic anisotropy and out-of-plane magnetization. The hysteresis characteristics in **d** and **e** indicate the non-volatile electrical toggling between two contrasting magnetization states. The error bars represent the standard deviation from the mean of 15 repetitive data acquisitions.

(Fig. 2a–d), we can infer that the transition from magnetoelectrically active to inactive regimes probably occurs at about 5L- or 6L-$Cr_2Ge_2Te_6$. Such a transition should not be abrupt but gradual, and the transition in the few-layer regime agrees with the interfacial nature of the magnetoelectric coupling that primarily arises from the interfacial wavefunction overlap.

Electrical toggling between two magnetization states

The above results demonstrate the efficient electrical control of the magnetic hysteresis characteristics of 2D $Cr_2Ge_2Te_6$. Next, we will examine whether voltages can directly toggle between distinct magnetization states (that is, without the need for sweeping magnetic fields), which holds direct technological relevance to useful devices[8,9,19,37]. Figure 4a shows the magnetic hysteresis of the 2L-$Cr_2Ge_2Te_6$ device that has already been trained into the ON state (that is, with an opened magnetic hysteresis loop). The voltage is then swept as a static magnetic field of ±30 mT is applied (at ±30 mT, the device is magnetically saturated) and as a static magnetic field of ±9 mT is applied (at ±9 mT, the device is magnetically unsaturated). At ±30 mT (Fig. 4b,c), the RMCD of 2L-$Cr_2Ge_2Te_6$ does not show a noticeable response to sweeping V_{EF} between −14 and +14 V. In the magnetically saturated regions, the spin orientation is strongly pinned normal to the crystal plane by the externally applied magnetic fields, and thus, the FE effect on magnetic anisotropy cannot overcome the magnetic alignment to the external field.

However, at ±9 mT (Fig. 4d,e) when the $Cr_2Ge_2Te_6$ magnetization is unsaturated, the voltage dependence of RMCD exhibits an electrical hysteresis. As shown in Fig. 4d, the RMCD abruptly changes when V_{EF} is swept down below −5 V or up above +5 V. Note that the coercive V_{EF} value of 5 V here agrees with the coercive V_{EF} value in Fig. 3, indicating that the observed magnetization control (Fig. 4d) arises from the interfacial multiferroic effect. Interestingly, the electrical hysteresis under +9 mT magnetic field (Fig. 4e) is opposite to that under −9 mT (Fig. 4d). When the out-of-plane magnetic field is not strong enough to completely pin the spin orientation, the interfacial multiferroic effect on magnetic anisotropy can compete with the Zeeman energy, leading to the ferroelectrically modulated magnetic anisotropy and out-of-plane magnetization.

Conclusions

We have reported the non-volatile electrical control of 2D magnetism in 2D-$Cr_2Ge_2Te_6$/P(VDF-TrFE) multiferroic heterostructures. Magnetic hysteresis in insulating 2D $Cr_2Ge_2Te_6$ can be opened and completely closed by applying ±5 V voltages across the multiferroic heterostructures due to strong interfacial magnetoelectric coupling. The multiferroic modulation of magnetic anisotropy in 2D $Cr_2Ge_2Te_6$ leads to non-volatile electrical toggling between two magnetization states. Our demonstration of low-voltage, non-volatile control of 2D MIs could be of use in the development of nanoscale spintronic, magnonic and magneto-optical applications[38].

Methods

Sample preparation

Atomically thin $Cr_2Ge_2Te_6$ samples were mechanically exfoliated from bulk crystals onto 260-nm-thick SiO_2/Si substrates, and the thicknesses of the as-exfoliated 2D $Cr_2Ge_2Te_6$ samples were identified by the optical contrast relative to the substrate and confirmed by AFM after all the device measurements. The samples were prepared and stored in a glovebox with oxygen and moisture levels below 0.1 ppm.

Device assembly

Multiferroic heterostructure devices were prepared by spin coating a thin film of P(VDF-TrFE) onto $Cr_2Ge_2Te_6$ flakes. The P(VDF-TrFE) with a molar ratio of 70/30 was dissolved in anhydrous

N,*N*-dimethylformamide (99.8%) to make a 2.5 wt% solution. The 50-nm-thick P(VDF-TrFE) thin film can be obtained by spin coating at 3,000 rpm for 30 s. The co-polymer film was then dried at 80 °C for 10 min and further annealed in the glovebox to improve the crystallinity. A 20-nm-thick transparent ITO was deposited by electron-beam evaporation to cover the multiferroic heterostructure as a transparent electrode. Another metallic contact (Cr (5 nm) and Au (50 nm)) for wire bonding was thermally evaporated on a side region of the ITO, which does not block the probing laser. A highly p-doped Si substrate served as the bottom electrode for all the devices, except for the redesigned device shown in Supplementary Fig. 8 where a graphite bottom electrode on SiO_2 was adopted (Supplementary Fig. 8 and Note). The devices were mounted on a dual in-line socket sample stage with silver paste, with both top and bottom electrodes wire-bonded to sockets for electrical connections.

RMCD characterization

The RMCD characterizations of our samples were conducted in a Montana closed-cycle cryostat down to 4 K and up to 300 mT in the out-of-plane direction. A 633 nm He–Ne laser served as the excitation, which was focused onto a sub-micrometre spot on the sample (optical power, ~7 μW) via a ×50 objective with 0.5 numerical aperture. The reflected light was collected by the same objective and detected by a photodiode. A chopper and photoelastic modulator were used to modulate the intensity and helicity/polarization of the excitation beam, respectively. The RMCD was determined by the ratio between the a.c. signal at 50 kHz (modulated by the photoelastic modulator) and the low-frequency a.c. signal at 237 Hz (modulated by the chopper) of the reflected light intensity, simultaneously measured by two different lock-in amplifiers. The phase of the 50 kHz a.c. signal was analysed to reflect the magnetization switching in the magnetic-field-dependent study of the redesigned device with a graphite bottom electrode.

Data availability

The data that support the plots within this paper and other findings of this study are available from the corresponding author upon reasonable request.

Code availability

The codes used for plotting the data are available from the corresponding author upon reasonable request.

References

1. Chumak, A. V., Vasyuchka, V. I., Serga, A. A. & Hillebrands, B. Magnon spintronics. *Nat. Phys.* **11**, 453–461 (2015).
2. Neusser, S. & Grundler, D. Magnonics: spin waves on the nanoscale. *Adv. Mater.* **21**, 2927–2932 (2009).
3. Kajiwara, Y. et al. Transmission of electrical signals by spin-wave interconversion in a magnetic insulator. *Nature* **464**, 262–266 (2010).
4. Cornelissen, L. J., Liu, J., Duine, R. A., Youssef, J. B. & van Wees, B. J. Long-distance transport of magnon spin information in a magnetic insulator at room temperature. *Nat. Phys.* **11**, 1022–1026 (2015).
5. Subkhangulov, R. R. et al. Terahertz modulation of the Faraday rotation by laser pulses via the optical Kerr effect. *Nat. Photon.* **10**, 111–114 (2016).
6. Khazanov, E. et al. Effect of terbium gallium garnet crystal orientation on the isolation ratio of a Faraday isolator at high average power. *Appl. Opt.* **41**, 483–492 (2002).
7. Yoshida, H. et al. Optical properties and Faraday effect of ceramic terbium gallium garnet for a room temperature Faraday rotator. *Opt. Express* **19**, 15181–15187 (2011).
8. Chu, Y.-H. et al. Electric-field control of local ferromagnetism using a magnetoelectric multiferroic. *Nat. Mater.* **7**, 478–482 (2008).
9. Spaldin, N. A. & Ramesh, R. Advances in magnetoelectric multiferroics. *Nat. Mater.* **18**, 203–212 (2019).
10. Baek, S. H. et al. Ferroelastic switching for nanoscale non-volatile magnetoelectric devices. *Nat. Mater.* **9**, 309–314 (2010).
11. Manipatruni, S. et al. Scalable energy-efficient magnetoelectric spin–orbit logic. *Nature* **565**, 35–42 (2019).
12. Mankalale, M. G. et al. CoMET: composite-input magnetoelectric-based logic technology. *IEEE J. Explor. Solid-State Computat.* **3**, 27–36 (2017).
13. Gong, C. et al. Discovery of intrinsic ferromagnetism in two-dimensional van der Waals crystals. *Nature* **546**, 265–269 (2017).
14. Huang, B. et al. Layer-dependent ferromagnetism in a van der Waals crystal down to the monolayer limit. *Nature* **546**, 270–273 (2017).
15. Heron, J. T. et al. Electric-field-induced magnetization reversal in a ferromagnet-multiferroic heterostructure. *Phys. Rev. Lett.* **107**, 217202 (2011).
16. Novoselov, K. S., Mishchenko, A., Carvalho, A. & Castro Neto, A. H. 2D materials and van der Waals heterostructures. *Science* **353**, aac9439 (2016).
17. Geim, A. K. & Grigorieva, I. V. Van der Waals heterostructures. *Nature* **499**, 419–425 (2013).
18. Si, M., Liao, P.-Y., Qiu, G., Duan, Y. & Ye, P. D. Ferroelectric field-effect transistors based on MoS_2 and $CuInP_2S_6$ two-dimensional van der Waals heterostructure. *ACS Nano* **12**, 6700–6705 (2018).
19. Ohno, H. et al. Electric-field control of ferromagnetism. *Nature* **408**, 944–947 (2000).
20. Dobrowolska, M. et al. Controlling the Curie temperature in (Ga,Mn)As through location of the Fermi level within the impurity band. *Nat. Mater.* **11**, 444–449 (2012).
21. Weisheit, M. et al. Electric field-induced modification of magnetism in thin-film ferromagnets. *Science* **315**, 349–351 (2007).
22. Duan, C. G. et al. Surface magnetoelectric effect in ferromagnetic metal films. *Phys. Rev. Lett.* **101**, 137201 (2008).
23. Huang, B. et al. Electrical control of 2D magnetism in bilayer CrI_3. *Nat. Nanotechnol.* **13**, 544–548 (2018).
24. Jiang, S., Li, L., Wang, Z., Mak, K. F. & Shan, J. Controlling magnetism in 2D CrI_3 by electrostatic doping. *Nat. Nanotechnol.* **13**, 549–553 (2018).
25. Wang, Z. et al. Electric-field control of magnetism in a few-layered van der Waals ferromagnetic semiconductor. *Nat. Nanotechnol.* **13**, 554–559 (2018).
26. Gong, C., Kim, E. M., Wang, Y., Lee, G. & Zhang, X. Multiferroicity in atomic van der Waals heterostructures. *Nat. Commun.* **10**, 2657 (2019).
27. Qi, J., Wang, H., Chen, X. & Qian, X. Two-dimensional multiferroic semiconductors with coexisting ferroelectricity and ferromagnetism. *Appl. Phys. Lett.* **113**, 043102 (2018).
28. Nakhmanson, S. M., Rabe, K. M. & Vanderbilt, D. Polarization enhancement in two- and three-component ferroelectric superlattices. *Appl. Phys. Lett.* **87**, 102906 (2005).
29. Liu, F. et al. Room-temperature ferroelectricity in $CuInP_2S_6$ ultrathin flakes. *Nat. Commun.* **7**, 12357 (2016).
30. Wu, D. et al. Thickness-dependent dielectric constant of few-layer In_2Se_3 nanoflakes. *Nano Lett.* **15**, 8136–8140 (2015).
31. Chen, X., Han, X. & Shen, Q.-D. PVDF-based ferroelectric polymers in modern flexible electronics. *Adv. Electron. Mater.* **3**, 1600460 (2017).
32. Neese, B. et al. Large electrocaloric effect in ferroelectric polymers near room temperature. *Science* **321**, 821–823 (2008).
33. Nemes-Incze, P., Osváth, Z., Kamarás, K. & Biró, L. P. Anomalies in thickness measurements of graphene and few layer graphite crystals by tapping mode atomic force microscopy. *Carbon* **46**, 1435–1442 (2008).

34. Salahuddin, S. & Datta, S. Use of negative capacitance to provide voltage amplification for low power nanoscale devices. *Nano Lett.* **8**, 405–410 (2008).
35. Rajapitamahuni, A., Hoffman, J., Ahn, C. H. & Hong, X. Examining graphene field effect sensors for ferroelectric thin film studies. *Nano Lett.* **13**, 4374–4379 (2013).
36. Hu, J.-M., Chen, L.-Q. & Nan, C.-W. Multiferroic heterostructures integrating ferroelectric and magnetic materials. *Adv. Mater.* **28**, 15–39 (2016).
37. Matsukura, F., Tokura, Y. & Ohno, H. Control of magnetism by electric fields. *Nat. Nanotechnol.* **10**, 209–220 (2015).
38. Gong, C. & Zhang, X. Two-dimensional magnetic crystals and emergent heterostructure devices. *Science* **363**, eaav4450 (2019).

Acknowledgements

C.G. acknowledges support from the Air Force Office of Scientific Research under award no. FA9550-22-1-0349, Naval Air Warfare Center Aircraft Division under award no. N00421-22-1-0001, Army Research Laboratory under cooperative agreement no. W911NF-19-2-0181, National Science Foundation under award nos. CMMI-2233592 and 49100423C0011, and Northrop Grumman Mission Systems' University Research Program. I.Ž. acknowledges support from the Air Force Office of Scientific Research under award no. FA9550-22-1-0349 and National Science Foundation under award nos. CMMI-2233375 and ECCS-2130845. S.-J.G. acknowledges support from the National Natural Science Foundation of China under award no. 62274066. J.-P.W. acknowledges support from the Robert F. Hartmann Endowed Chair Professorship. M.A.S. and B.S.C. acknowledge support from the United States Air Force Office of Scientific Research LRIR 18RQCOR100 and AOARD-MOST grant no. F4GGA21207H002. B.S.C. further acknowledges the National Research Council Senior Fellowship award. C.G. is grateful for the fruitful discussions with J. Chang, R. Howell and Q. Zhang.

Author contributions

C.G. conceived and supervised the project. S.L. conducted the exfoliation of 2D samples and device fabrication with the assistance of T.X. S.L. and T.X. performed the RMCD measurements under the supervision of C.G., with the assistance of Z.S. for the Raman spectroscopic measurements. N.A.B. conducted the capacitance measurements under the supervision of A.L.F. T.E. carried out the AFM measurements under the supervision of M.O. T.Z. conducted the DFT calculations under the supervision of I.Ž. M.A.S. and B.S.C. synthesized the bulk single crystals of $Cr_2Ge_2Te_6$. S.-J.G. partially provided the understanding of the DFT method. J.-P.W. contributed to the potential spintronic-devices-related discussion. S.L. and C.G. analysed the data. S.L., J.L., X.Z. and C.G. wrote the paper. All the authors commented on the paper.

Competing interests

The authors declare no competing interests.

Additional information

Supplementary information The online version contains supplementary material available at https://doi.org/10.1038/s41928-023-00931-1.

Correspondence and requests for materials should be addressed to Cheng Gong.

Peer review information *Nature Electronics* thanks Manfred Fiebig and the other, anonymous, reviewer(s) for their contribution to the peer review of this work.